Journal of Solid State Chemistry **160,** 239–246 (2001)
doi:10.1006/jssc.2001.9230, available online at http://www.idealibrary.com on IDEAL®

On the Structural and Electronic Factors Governing the Magnetic Properties of the Hexagonal Perovskite-Type Oxides A_xBO_3 (A = Ca, Sr, Ba; B = Co, Ni)

M.-H. Whangbo,[1] H.-J. Koo, and K.-S. Lee[2]

Department of Chemistry, North Carolina State University, Raleigh, North Carolina 27695-8204

and

O. Gourdon, M. Evain, S. Jobic,[1] and R. Brec

Institut des Matériaux Jean Rouxel, Laboratoire de Chimie des Solides, 2 rue de la Houssinière, B.P. 32229, 44322 Nantes Cedex 03, France

Received February 12, 2001; accepted April 30, 2001; published online June 29, 2001

The hexagonal perovskite-type oxides A_xBO_3 (A = Ca, Sr, Ba; B = Co, Ni) consist of $(BO_3)_\infty$ chains made up of face-sharing BO_6 octahedra and BO_6 trigonal prisms. On the basis of molecular orbital calculations for their structural building blocks we examined why the transition metal atoms in the trigonal prisms of $Sr_{9/7}NiO_3$ and $Sr_{14/11}CoO_3$ occupy the positions away from their trigonal prism centers and why $Ba_{6/5}NiO_3$ and $Ca_{3/2}CoO_3$ exhibit apparently puzzling magnetic properties. Our analysis indicates that the structural building units of the $(BO_3)_\infty$ chains in these oxides adopt high-spin states to reduce the metal–metal σ-antibonding interactions between adjacent metal atoms as well as the on-site repulsion. This finding led us to predict the number of unpaired spins that the oxides $Sr_{9/7}NiO_3$, $Sr_{6/5}CoO_3$, and $Sr_{14/11}CoO_3$ are expected to have. © 2001 Academic Press

1. INTRODUCTION

Hexagonal perovskite-type oxides A_xBO_3 consist of infinite $(BO_3)_\infty$ and A_∞ chains. In the $(BO_3)_\infty$ chains of a short-period commensurate phase such as $Ca_{3/2}CoO_3$ (1), BO_6 octahedra alternate with BO_6 trigonal prisms by sharing triangular faces (Fig. 1a). In the infinite $(BO_3)_\infty$ chains of long-period commensurate phases such as $Ba_{6/5}NiO_3$ (2, 3), $Sr_{6/5}CoO_3$ (4) and $Sr_{14/11}CoO_3$ (5) several octahedra share their *trans* faces to form octahedral oligomers B_nO_{3n+3} (n = 2–4) and such oligomers alternate with single trigonal prisms along the chain direction (Figs. 1b and 1c). In the infinite $(BO_3)_\infty$ chains of incommensurate phases such as $Sr_{1.2872}NiO_3$ (6), the trigonal prisms and two types of octahedral oligomers, B_2O_9 and B_3O_{12}, occur randomly. For simplicity, $Sr_{1.2872}NiO_3$ is approximated by the commensurate structure $Sr_{9/7}NiO_3$ (6) (Fig. 1d). Analysis of the B–O bond lengths in $Sr_{9/7}NiO_3$ and $Sr_{14/11}CoO_3$ indicates (5, 6) that the oxidation states of the transition metal atoms in the octahedral (Oh) and trigonal prism (TP) BO_6 units are close to $+4$ and $+2$, respectively. (Here the term "oxidation state" is used from the viewpoint of the ionic electron counting scheme (7), which is an expedient way of determining the number of electrons in d-block energy levels.) This number is close to but not the same as the number of d-electrons on the metal, because the d-block levels are composed of metal d and ligand s/p orbitals. For example, $BaNiO_3$ consists of $(NiO_3)_\infty$ chains made up of only face-sharing NiO_6 octahedra. The ionic electron counting scheme suggests that the oxidation state of nickel is $+4$ in $BaNiO_3$, so that $BaNiO_3$ has six electrons per formula to fill its d-block bands. The nickel oxidation state of $BaNiO_3$ was reported to be close to $+3$ (8) on the basis of XPS and Mössbauer spectroscopy.

In $Sr_{9/7}NiO_3$ the nickel atom of each NiO_6 octahedron is at the Oh center. However, the nickel atom of each NiO_6 trigonal prism is located randomly at the centers of the three square-like faces (i.e., hereafter referred to as the square-planar (SP) centers) as well as at two off-centered positions on the 3-fold rotational axis displaced from the TP center by $\sim$0.12 Å (Fig. 2) (6). In $Sr_{14/11}CoO_3$ the TP cobalt atoms occupy the positions displaced from the TP center toward the SP centers. Unlike the case of $Sr_{9/7}NiO_3$, however, the two off-centered positions on the 3-fold rotational axis are not occupied (5). Observations similar to these are expected for $Ba_{6/5}NiO_3$ and $Sr_{6/5}CoO_3$ because the atomic

[1] To whom correspondence should be addressed.

[2] Permanent address: Department of Chemistry, The Catholic University of Korea, Puchon, Kyunggi-Do, South Korea 422-743.

0022-4596/01 $35.00
Copyright © 2001 by Academic Press
All rights of reproduction in any form reserved.

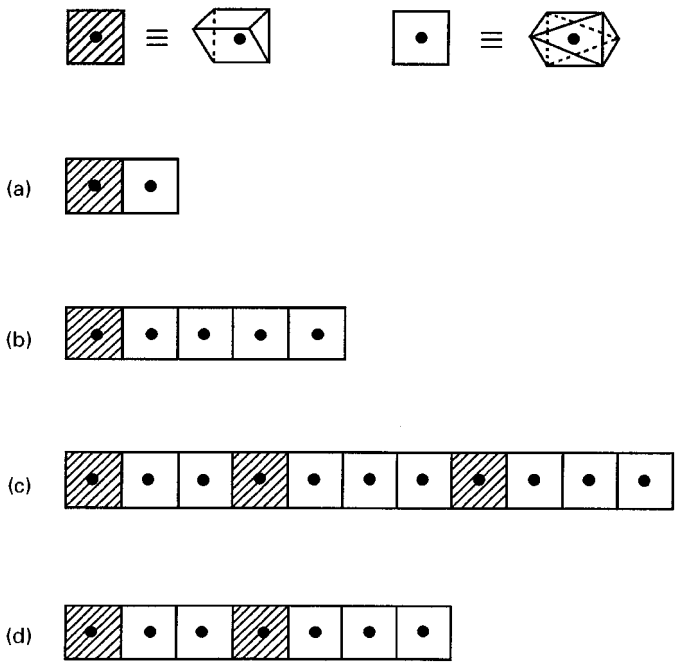

FIG. 1. Schematic representations of the BO_6 octahedra and BO_6 trigonal prisms that appear in the unit cells of the $(BO_3)_\infty$ chains in (a) $Ca_{3/2}CoO_3$, (b) $Ba_{6/5}NiO_3$ and $Sr_{6/5}CoO_3$, (c) $Sr_{14/11}CoO_3$, and (d) $Sr_{9/7}NiO_3$. The shaded squares represent BO_6 trigonal prisms, and the open squares the BO_6 octahedra.

displacement parameters (i.e., the thermal parameters) of their transition metal atoms are considerably larger at the BO_6 trigonal prisms than at the BO_6 octahedra (2, 4). So far there has been no systematic study concerning why the TP transition metal atoms in $Sr_{9/7}NiO_3$ and $Sr_{14/11}CoO_3$ occupy the positions away from the TP centers and what the answer to this question might imply about the magnetic properties of these oxides.

The compounds $Ba_{6/5}NiO_3$ and $Ca_{3/2}CoO_3$ present apparently puzzling magnetic properties. $Ba_{6/5}NiO_3$ was originally reported as $BaNi_{0.83}O_{2.5}$ (2), but the "$Ba_{6/5}NiO_3$" formulation was later shown to be the correct one (3). The $(NiO_3)_\infty$ chain of $Ba_{6/5}NiO_3$ has one Ni_4O_{15} octahedral tetramer and one NiO_6 trigonal prism (i.e., five nickel atoms) per unit cell (Fig. 1b). The effective magnetic moment μ_{eff} of $Ba_{6/5}NiO_3$ was determined to be $1.31\,\mu_B$ per formula unit (2), which is equivalent to about three spins per five nickel atoms according to the relationship $\mu_{eff} = \sqrt{n(n+2)}$, where n is the average number of spins per Ni. From the viewpoint of the electronic structure of an isolated NiO_6 octahedron, the $Ni^{4+}(d^6)$ cation at each Oh center would have no unpaired spin (Fig. 3a). Likewise, from the viewpoint of the electronic structure of an isolated NiO_6 trigonal prism, the $Ni^{2+}(d^8)$ cation in each trigonal prism would have two unparied spins if the cation lies on the 3-fold rotational axis (Fig. 3b), but no spin if the cation is located at the SP center (Fig. 3c). Consequently, with the occupancy ~ 0.2 for each of the three SP centers and two off-centered positions on the 3-fold axis in a TP, $Ba_{6/5}NiO_3$ is expected to have about one spin (~ 0.8 spin) per five nickel atoms, which is in disagreement with experiment.

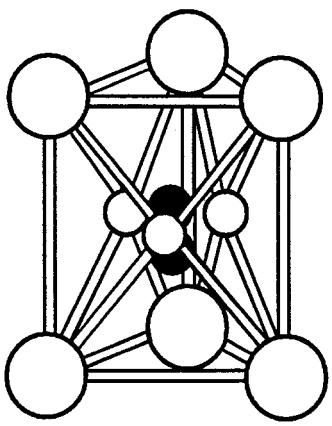

FIG. 2. Schematic representations of the Ni atom positions found in the NiO_6 trigonal prisms of $Sr_{9/7}NiO_3$. The large empty circles represent the oxygen atoms, the small empty circles the Ni atoms at the square-planar sites, and the small filled circles the Ni atoms at the two off-center positions (on the three-fold axis displaced from the trigonal prism center by ~ 0.12 Å).

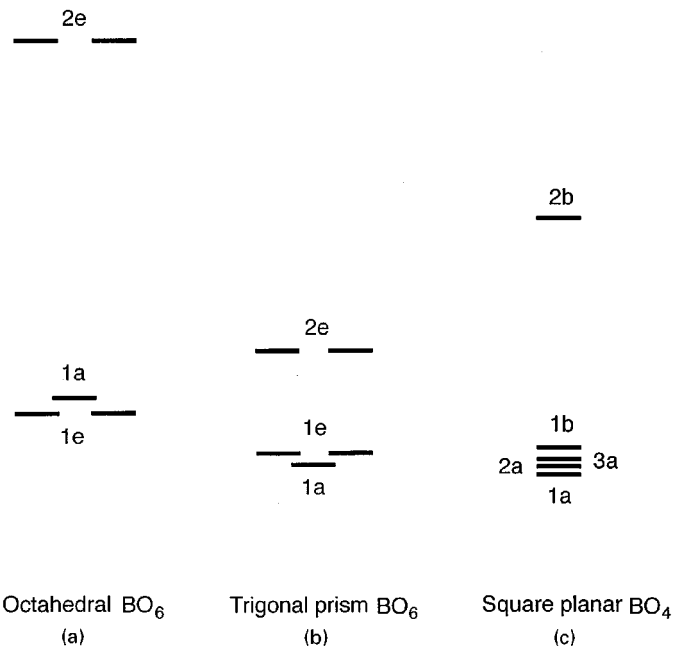

FIG. 3. Schematic representations of the d-block levels of (a) an octahedral BO_6, (b) a trigonal prism BO_6 with B at the trigonal prism center, and (c) a square planar BO_4 (i.e., BO_6 trigonal prism with B at one square planar center). The symmetry labels of the d-block levels in (a) and (b) are assigned with respect to the C_3 point symmetry group, and those in (c) with respect to the C_2 point symmetry group.

Moreover, examination of the Co–O bond lengths in $Ca_{3/2}CoO_3$ indicated (1) that the oxidation state of the Oh cobalt is considerably larger than that of the TP cobalt (i.e., $+3.25$ vs $+2.25$), and the average Co oxidation state is smaller than the value $+3$ required by the charge balance for $Ca_{3/2}CoO_3$. The latter is due most likely to the metal–metal bonding between adjacent Oh and TP cobalt atoms (Co–Co = 2.60 Å) (1). The magnetic properties of $Ca_{3/2}CoO_3$ have been the subject of several studies (9–13). According to the neutron diffraction study (9) of $Ca_{3/2}CoO_3$, the effective magnetic moments of the cobalt atoms at the Oh and TP sites are 0.08 ± 0.04 and $3.00 \pm 0.05\ \mu_B$, respectively. The study of Kageyama *et al.* (11) using oriented samples along the chain direction led to the conclusion that each Oh cobalt is practically nonmagnetic while each TP cobalt has about two spins. From the viewpoint of the electronic structure of an isolated CoO_6 octahedron, the Oh cobalt atom should exist as a $Co^{3+}(d^6)$ cation to be nonmagnetic (9). If so, the charge balance for $Ca_{3/2}CoO_3$ requires that each TP cobalt atom also exist as a $Co^{3+}(d^6)$ cation. This picture cannot explain why the TP cobalt possesses two spins and is in conflict with the oxidation states deduced from the crystal structure analysis (9).

In the present work we probe the questions and puzzling observations described above by analyzing the crystal and electronic structures of the oxides A_xBO_3. The objective of our study is to seek qualitative understanding that can lead to verifiable predictions. Two important structural/electronic features of these oxides will guide our analysis. One is that the $(BO_3)_\infty$ chains have short nearest-neighbor B–B distances. Provided that the local z-axis is taken along the 3-fold rotational axis of each $(BO_3)_\infty$ chain, the z^2 orbitals of the adjacent B atoms can overlap strongly through the shared face. When the z^2 orbital of an isolated BO_6 polyhedron (i.e., trigonal prism or octahedron) is doubly occupied, it acts as a lone-pair orbital. However, short nearest-neighbor B–B distances of a $(BO_3)_\infty$ chain can cause significant two-orbital four-electron destabilization (14) if the z^2 orbitals of the associated BO_6 polyhedra are each doubly occupied. The other feature is that when the metal atom of a BO_6 polyhedron lies on the 3-fold rotational axis, its d-block levels are grouped into one nondegenerate (i.e., the z^2 orbital) and two doubly degenerate levels (Figs. 3a and 3b). A doubly degenerate level of the BO_6 polyhedra can act as a source of two unpaired spins when it is occupied by two electrons. In the following the two structural/electronic features will be found to play a crucial role in determining magnetic properties of the oxides A_xBO_3.

2. THEORETICAL CONSIDERATIONS

In general, the electronic properties of extended solids are described in terms of electronic band structure calculations. Although the oxides A_xBO_3 are extended solids, we will examine their electronic properties in terms of the molecular orbital structures calculated for their structural building blocks. As illustrated in Fig. 4, the d-block bands of an extended solid are related to the d-block levels calculated for its structural building block such that the mean value of a d-block band is approximately equal to the corresponding d-block level. Furthermore, a magnetic state of an extended solid with several unpaired spins per unit cell is represented by the electron configuration in which all the levels of the corresponding bands are each singly filled (e.g., the top two bands of Fig. 4b) (15, 16). Consequently, the relative stabilities of the various spin states of an extended solid can be estimated by examining those of the corresponding states of its structural building blocks. Since our study is aimed at gaining qualitative insight into the magnetic properties of the oxides A_xBO_3, the electronic structure calculations needed for our analysis will be based on the extended Hückel method (17, 18) using the parameters of the atomic orbitals listed in Table 1. On a qualitative level, the deficiency of this one-electron method in dealing with the stability difference between different-spin electronic states can be corrected by introducing electron–electron repulsion in terms of effective on-site repulsion U (15, 16, 19). This approach is similar in spirit to describing strongly correlated solids (i.e., magnetic solids) in terms of a phenomenological Hamiltonian (19, 20), and also to describing them in terms of electronic band structure calculations plus on-site repulsion correction (21, 22). Recent studies have shown that the trends in the anisotropic spin exchange interactions of magnetic solids are well reproduced in terms of spin–orbital interaction energies calculated for their spin dimers using the extended Hückel method (23–29). Concerning why this

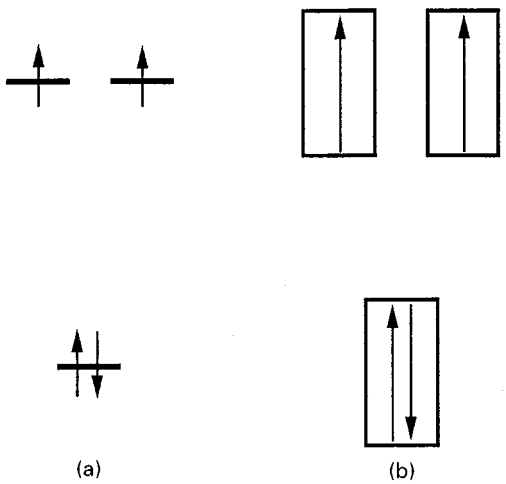

FIG. 4. Schematic correlation diagram between the d-block bands of an extended solid and the d-block levels of its structural fragment: (a) the d-block levels and (b) the d-block bands. An energy band representing a localized electron has all its band levels singly filled. The diagram shows two localized electrons (i.e., two unpaired spins) per unit cell.

TABLE 1

Exponents ζ_i and Valence Shell Ionization Potentials H_{ii} of Slater-Type Orbitals χ_i used for Extended Hückel Tight-Binding Calculation[a]

Atom	χ_i	H_{ii}(eV)	ζ_i	c_1[b]	ζ_i'	c_2[b]
Ni	4*s*	− 9.17	1.825	1.0		
Ni	4*p*	− 5.15	1.125	1.0		
Ni	3*d*	− 13.5	5.750	0.5683	2.000	0.6292
Co	4*s*	− 9.21	2.000	1.0		
Co	4*p*	− 5.29	2.000	1.0		
Co	3*d*	− 13.2	5.550	0.5679	2.100	0.6059
O	2*s*	− 32.3	2.275	1.0		
O	2*p*	− 14.8	2.275	1.0		

[a] H_{ii}'s are the diagonal matrix elements $\langle\chi_i|H^{\text{eff}}|\chi_i\rangle$, where H^{eff} is the effective Hamiltonian. In our calculations of the off-diagonal matrix elements $H^{\text{eff}} = \langle\chi_i|H^{\text{eff}}|\chi_j\rangle$, the weighted formula was used. See: Ammeter, J.; Bürgi, H.-B.; Thibeault, J.; Hoffmann, R., *J. Am. Chem. Soc.* 1978, 100, 3686.

[b] Contraction coefficients used in the double-ζ Slater-type orbital.

simple method can be used to discuss the electronic properties of strongly correlated systems, the reader is referred to a recent review (30).

3. IMPLICATIONS OF THE METAL ATOM OCCUPATION AT THE NON CENTRAL SITES OF THE TRIGONAL PRISMS IN $Sr_{9/7}NiO_3$ AND $Sr_{14/11}CoO_3$

3.1. $Sr_{9/7}NiO_3$

In the hexagonal perovskite-type phases A_xBO_3, the BO_6 octahedra are slightly distorted from a regular octahedron, while the BO_6 trigonal prisms are slightly distorted from a true trigonal prism such that the two O_3 triangles are not eclipsed but make a dihedral angle of about 10–15 degrees for small A^{2+} cations such as Ca^{2+}. Figure 3a depicts the *d*-level ordering calculated for an isolated NiO_6 octahedron of $Sr_{9/7}NiO_3$, and Fig. 3b that for an isolated NiO_6 trigonal prism of $Sr_{9/7}NiO_3$ with the nickel atom at the TP center. The symmetry labels of the *d*-block levels in Figs. 3a and 3b are assigned with respect to the C_3 point symmetry group. For the NiO_6 octahedron, the 1*a* and 1*e* levels constitute the t_{2g}-block levels, and the 2*e* levels the e_g-block levels (Fig. 3a). The 1*a* levels of the NiO_6 octahedron and the NiO_6 trigonal prism are mainly represented by the nickel z^2 orbitals. The energy split between the lower three and the upper two levels is much larger for the NiO_6 octahedron than for the NiO_6 trigonal prism (3.5 vs 1.0 eV). The 2*e* levels of the NiO_6 trigonal prism lie close to the 1*e* levels of the NiO_6 octahedron (0.5 eV above). Figure 3c shows the *d*-level ordering of the NiO_6 trigonal prism calculated for the case when the nickel atom is located at one SP center. In Fig. 3c the symmetry labels of the *d*-block levels are assigned with respect to the C_2 point symmetry group (the 2-fold rotational axis is perpendicular to the 3-fold rotational axis), and the energy split between the highest two levels is large (about 2.2 eV).

In $Sr_{9/7}NiO_3$, each octahedron has a $Ni^{4+}(d^6)$ cation, and each trigonal prism a $Ni^{2+}(d^8)$ cation. Therefore, according to the relative energy orderings of the *d*-block levels shown in Figs. 3a–3c, it is expected that a nickel atom at the Oh center has the $S = 0$ configuration Φ_{oh}, that at the TP center the $S = 1$ configuration Φ_{tp}, and that at the SP center the $S = 0$ configuration Φ_{sp}.

$$\Phi_{oh} = (1a)^2(1e)^4$$
$$\Phi_{tp} = (1a)^2(1e)^4(2e)^2 \qquad [1]$$
$$\Phi_{sp} = (1a)^2(2a)^2(3a)^2(1b)^2.$$

Our calculations for the $(NiO_6)^{10-}$ trigonal prism show that when the nickel atom lies on the 3-fold rotational axis, the most stable position of the nickel atom is the TP center, and displacing the nickel atom away from the TP center along the 3-fold axis requires a very small amount of energy (e.g., 0.09 eV for the displacement of 0.25 Å). Consequently, the nickel atom in each NiO_6 trigonal prism of $Sr_{9/7}NiO_3$ would occupy the region of the 3-fold rotational axis between the two off-centered positions. Our calculations also show that the $S = 0$ state Φ_{sp} is more stable than the $S = 1$ state given Φ_{tp} by 2.0 eV. However, the total energy of a given state by extended Hückel calculations does not include the effect of electron–electron repulsion. Thus, the relative energies of two states different in the total spin quantum number cannot be compared on the basis of their one-electron energies determined by extended Hückel calculations (15, 30). The $S = 0$ state Φ_{sp} consists of only completely filled *d*-block levels, while the $S = 1$ state Φ_{tp} has two half-filled *d*-block levels. Therefore, the extent of electron–electron repulsion is larger in Φ_{sp} than in Φ_{tp}. This difference in electron–electron repulsion can be discussed in terms of the phenomenological parameter, on-site repulsion *U* (19). The effective on-site repulsion in Φ_{sp} (i.e., U_{sp}) should then be larger than that in Φ_{tp} (i.e., U_{tp}). Since the SP centers are almost equally occupied as are the region of the 3-fold rotational axis between the two off-centered positions, the $S = 0$ state Φ_{sp} would be comparable in energy to the $S = 1$ state Φ_{tp}, thereby suggesting that $U_{sp} - U_{tp} \approx 2$ eV. The importance of on-site repulsion will be discussed further in Sections 4 and 5.

3.2. $Sr_{14/11}CoO_3$

Our calculations reveal that the *d*-block levels of the CoO_6 octahedra, CoO_6 trigonal prism, and CoO_4 square are split as in the case of the nickel analogs shown in Figs.

3a–3c. Analysis of the Co–O bond lengths of $Sr_{14/11}CoO_3$ indicated that the Oh and TP sites have $Co^{4+}(d^5)$ and $Co^{2+}(d^7)$ cations, respectively (5). Therefore, the cobalt atoms at the Oh, TP, and SP centers are expected to have the $S = \frac{1}{2}$ configurations Ψ_{oh}, Ψ_{tp}, and Ψ_{sp}, respectively.

$$\begin{aligned}\Psi_{oh} &= (1a)^2(1e)^3 \text{ or } (1a)^1(1e)^4\\ \Psi_{tp} &= (1a)^2(1e)^4(2e)^1\\ \Psi_{sp} &= (1a)^2(2a)^2(3a)^2(1b)^1.\end{aligned} \qquad [2]$$

Our calculations for $(CoO_6)^{10-}$ show that the state Ψ_{sp} is only slightly more stable than Ψ_{tp} (by 0.39 eV), because the $1b$ level is singly filled. This explains why the TP cobalt atoms of $Sr_{14/11}CoO_3$ occupy the positions only slightly displaced from the TP center toward the SP center, since the electronic energy gain is not strong enough to overcome the stress associated with occupying the SP position. Furthermore, the Ψ_{tp} state should have a Jahn–Teller instability since the degenerate $2e$ levels are unequally filled (14). Thus, each TP cobalt atom of $Sr_{14/11}CoO_3$ should avoid any position on the 3-fold rotational axis. Notice that the $S = \frac{3}{2}$ state $\Psi'_{tp} = (1a)^2(1e)^3(2e)^2$ is another conceivable open-shell configuration each CoO_6 trigonal prism may adopt. This state also possesses a Jahn–Teller instability.

4. IMPLICATIONS OF THE SPIN DISTRIBUTIONS IN $Ba_{6/5}NiO_3$ AND $Ca_{3/2}CoO_3$ ON THE METAL–METAL σ-ANTIBONDING AND ON-SITE REPULSION

So far our discussion has neglected the orbital interactions between adjacent octahedra and trigonal prisms in the $(BO_3)_\infty$ chains. If we consider the electronic structures of isolated BO_6 octahedra and isolated BO_6 trigonal prisms, then their z^2 orbitals would be described as lone-pair orbitals. In general, the nearest-neighbor B–B distances of the $(BO_3)_\infty$ chains are rather short so that there will be significant overlap between nearest-neighbor z^2 orbitals. Figures 5a–5d show the qualitative patterns of the σ-type energy levels of the B_nO_{3n+3} ($n = 2$–5) oligomers that result from their z^2 orbitals. For even $n(=2, 4)$ the σ-levels are split into bonding and antibonding levels, while for odd $n(=3, 5)$ the σ-levels are split into bonding, nonbonding, and antibonding levels. It is energetically unfavorable to occupy the σ-antibonding levels, and this can have important consequences on the structural and magnetic properties of hexagonal perovskite-type oxides A_xBO_3, as will be discussed below.

4.1. $Ba_{6/5}NiO_3$

Our discussion of $Sr_{9/7}NiO_3$ in Section 3.1 showed that only the TP nickel atoms on the 3-fold rotational axis provide spins (i.e., two spins per nickel), and only about half ($\sim$40%) the TP nickel atoms lie on the 3-fold axis. A similar situation is expected for the TP nickel atoms of $Ba_{6/5}NiO_3$ because the crystal structure study of $Ba_{6/5}NiO_3$ shows large atomic displacement parameters for the TP nickel atom (3). There is then about one ($\sim$0.8) spin per five nickel atoms in $Ba_{6/5}NiO_3$. Experimentally, $Ba_{6/5}NiO_3$ is found to have about three spins per five nickel atoms, as pointed out earlier. Consequently, there must be an additional source of spin in $Ba_{6/5}NiO_3$ that creates two more spins per five nickel atoms.

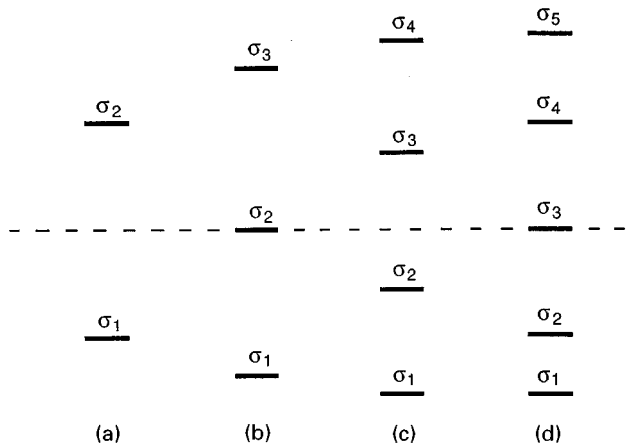

FIG. 5. Schematic representations of the σ levels expected from the z^2 orbitals of (a) the B_2O_9 dimer, (b) the B_3O_{12} trimer, (c) the B_4O_{15} tetramer, and (d) the B_5O_{18} pentamer of the $(BO_3)_\infty$ chains in hexagonal perovskite-type phase A_xBO_3. The horizontal dashed line refers to the nonbonding level.

We note that the Ni–Ni distances in the $(Ni_4O_{15})^{14-}$ octahedral tetramer are quite short (i.e., 2.34, 2.56, 2.34 Å) compared with the Ni–Ni distance between adjacent Oh and TP centers (2.81 Å). Hence, the σ-interactions between octahedra are expected to be much stronger than those between an octahedron and a trigonal prism. To a first approximation, the latter may then be neglected. The four z^2 orbitals of the octahedral tetramer form two σ-bonding levels and two σ-antibonding levels (Fig. 5c). Our calculations show that the two σ-antibonding levels are the two highest-lying ones of the 12 t_{2g}-block levels of the tetramer, and that the HOMO level σ_4 lies 1.4 eV below the LUMO level $2e_1$, i.e., the lowest-lying one of the eight e_g-block levels (Fig. 6a). Thus, the HOMO–LUMO gap is significantly smaller in the octahedral tetramer $(Ni_4O_{15})^{14-}$ than in the $(NiO_6)^{8-}$ octahedron (1.4 vs 2.2 eV). From the one-electron viewpoint, the ground state of the octahedral tetramer $(Ni_4O_{15})^{14-}$ would be the $S = 0$ state $\Phi_{cs} = (\cdots)(\sigma_3)^2(\sigma_4)^2$. Here the symbol $(\cdots)$ means that all the levels lying below σ_3 are completely filled, and the suffix "cs" refers to closed-shell. The HOMO σ_4 is nondegenerate, while the LUMO $2e_1$ is doubly degenerate. Thus, the promotion of two

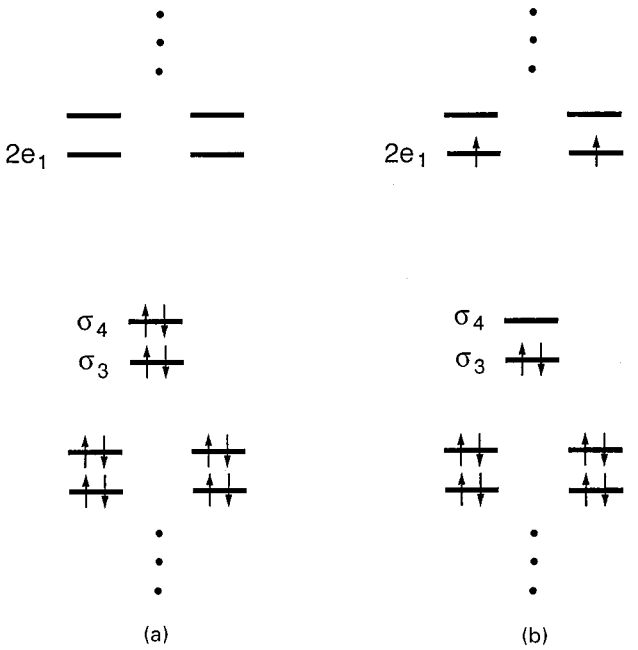

FIG. 6. Schematic representations of the orbital occupancies for (a) the $S = 0$ state Φ_{cs} and (b) the $S = 1$ state Φ_{os} of the octahedral tetramer $(Ni_4O_{15})^{14-}$ in $Ba_{6/5}NiO_3$.

electrons from the HOMO to the LUMO will generate two additional spins in each octahedral tetramer unit. In the resulting $S = 1$ state $\Phi_{os} = (\cdots)(\sigma_3)^2(2e_1)^2$ (Fig. 6b), where the suffix "os" refers to open-shell, and the extent of metal–metal σ-antibonding and that of effective on-site repulsion are both reduced. In addition, the promotion energy required for the electron transfer is reduced because the HOMO level is raised considerably due to the σ-antibonding. Thus, the experimental observation that there are three spins per five nickel atoms in $Ba_{6/5}NiO_3$ suggests that the $S = 1$ state Φ_{os} is more stable than the $S = 0$ state Φ_{cs} in the octahedral tetramer.

The $(NiO_3)_\infty$ chains of $BaNiO_3$ are made up of only face-sharing NiO_6 octahedra with the nearest-neighbor Ni–Ni distance of 2.41 Å (31). From the viewpoint of one-electron electronic structure, the oxidation state $Ni^{4+}(d^6)$ in $BaNiO_3$ implies that the t_{2g}-block bands of $BaNiO_3$ are completely filled while the e_g-block bands are empty. The band gap between the two bands is calculated to be ~ 1.0 eV according to our electronic band structure calculations based on the extended Hückel method (18, 32). Thus, the one-electron picture, unlike the case of $Ba_{6/5}NiO_3$, readily explains the diamagnetic (8, 33) and semiconducting (34) properties of $BaNiO_3$. It is interesting to speculate whether this difference orginates from the structural difference in the $(NiO_3)_\infty$ chains of the two compounds; the Ni atoms are uniformly distributed in $BaNiO_3$, but not in $Ba_{6/5}NiO_3$.

4.2. $Ca_{3/2}CoO_3$

As already mentioned, the assignment of the oxidation state $Co^{3+}(d^6)$ for the Oh and TP cobalt atoms is incompatible with the available experimental results (9). By analogy with $Sr_{14/11}CoO_3$, therefore, one may assume that the Oh and TP cobalt centers of $Ca_{3/2}CoO_3$ have $Co^{4+}(d^5)$ and $Co^{2+}(d^7)$ cations, respectively. On the basis of the electronic structures of an isolated CoO_6 octahedron and an isolated CoO_6 trigonal prism, it is also difficult to explain the nonmagnetic nature of the Oh cobalt as well as the presence of two spins on the TP cobalt (11). This difficulty arises because the effect of the interaction between the z^2 orbitals of adjacent Oh and TP cobalt atoms, which is strong due to the short Co–Co distance (i.e., 2.60 Å), cannot be neglected.

A dimer unit $(Co_2O_9)^{12-}$ of $Ca_{3/2}CoO_3$ contains one CoO_6 octahedron and one CoO_6 trigonal prism. The d-block energy levels calculated for such a dimer unit are presented in Fig. 7a. The two z^2 orbitals of the Oh and TP cobalt atoms form the σ-bonding and σ-antibonding levels (Fig. 5a). The $1e$ orbitals of the Oh and TP cobalt atoms lead to the $1e_t$ and $1e_o$ levels of the dimer. The $1e_t$ level is represented mainly by the $1e$ orbital of the TP cobalt, and the $1e_o$ level by the $1e$ orbital of the Oh cobalt. Likewise, the $2e$ orbitals of the Oh and TP cobalt atoms give rise to the $2e_t$ and $2e_o$ levels of the dimer. The $2e_t$ level is represented mainly by the $2e$ orbital of the TP cobalt, and the $2e_o$ level by the $2e$ orbital of the Oh cobalt. The LUMO $2e_t$ lies 0.8 eV above the HOMO σ_2. From the viewpoint of the one-electron energy, the $S = 0$ state $\Psi_{cs} = (\sigma_1)^2(1e_t)^4(1e_o)^4(\sigma_2)^2$ would be the ground state (Fig. 7a). The transfer of the two electrons from the nondegenerate σ_2 to the doubly

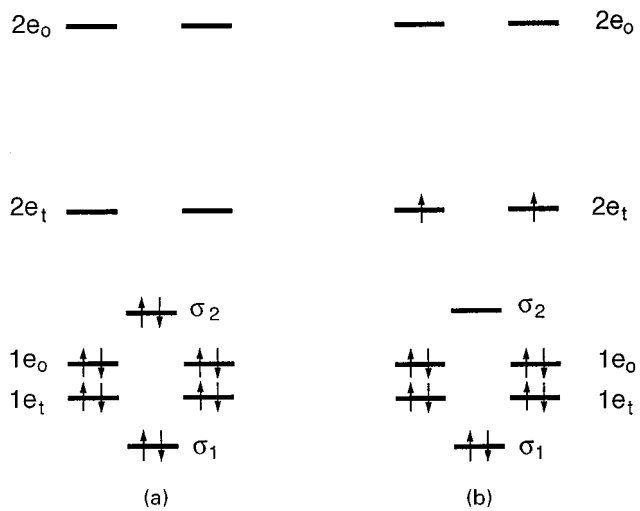

FIG. 7. Schematic representations of the orbital occupancies for (a) the $S = 0$ state Ψ_{cs} and (b) the $S = 1$ state Ψ_{os} of the dimer unit $(Co_2O_9)^{12-}$ in $Ca_{3/2}CoO_3$.

degenerate $2e_t$ gives rise to the $S = 1$ state $\Psi_{os} = (\sigma_1)^2(1e_t)^4(1e_o)^4(2e_t)^2$ (Fig. 7b).

Compared with the $S = 0$ state Ψ_{cs}, the extent of metal–metal σ-antibonding and that of effective on-site repulsion are both reduced in the $S = 1$ state Ψ_{os}. Since the $2e_t$ level is mainly composed of the $2e$ level of the TP cobalt, the $S = 1$ state Ψ_{os} predicts nearly two spins at the TP cobalt and almost no spin at the Oh cobalt, in agreement with the conclusion of Kageyama *et al.* (11). The σ-bonding level σ_1 of the dimer unit $(Co_2O_9)^{12-}$ is composed of the z^2 orbitals of the TP and Oh cobalt atoms. Since the $1a$ level of the TP cobalt lies lower than that of the Oh cobalt, the σ_1 level has a slightly greater contribution from the z^2 orbital of the TP cobalt. For the sake of simple electron counting, the z^2 orbitals of the TP and Oh cobalt atoms may be assumed to contribute equally to the σ-bonding level σ_1. The $S = 1$ state Ψ_{os} then predicts that the oxidations states of the Oh and TP cobalt atoms are close to $+4$ and $+2$, respectively. This is consistent with the experimental finding that the Oh cobalt has a considerably higher oxidation state than does the TP cobalt. In short, the apparently puzzling magnetic properties of $Ca_{3/2}CoO_3$ are readily accounted for if the $S = 1$ state Ψ_{os} is more stable than the $S = 0$ state Ψ_{cs}. Since the σ-antibonding level σ_2 is unoccupied in Ψ_{os}, this state also predicts that the nearest-neighbor Co–Co distance should be short (i.e., 2.60 Å), in agreement with experiment. In addition, the $S = 1$ state Ψ_{os} does not have unequally filled degenerate levels and hence is not subject to Jahn–Teller instability, which is consistent with the finding that the TP cobalt atoms lie on the 3-fold rotational axis (1).

$BaCoCO_3$ consists of infinite $(CoO_3)_\infty$ chains that are made up of only face-sharing CoO_6 octahedra with the nearest-neighbor Co–Co distance of 2.38 Å (31). Spin-polarized electronic band structure calculations for $BaCoO_3$ show that it is a magnetic metal, but the electrical resistivity and magnetic susceptibility measurements suggested that the electrons of $BaCoO_3$ are localized by the Anderson mechanism (i.e., electron localization due to the presence of random potentials) (35). At present the cause for this Anderson localization is unknown. It is tempting to speculate whether the random potentials of this compound are caused by a small number of trigonal prisms that occur randomly in the $(CoO_3)_\infty$ chains.

5. PROBABLE NUMBER OF UNPAIRED SPINS IN $Sr_{9/7}NiO_3$, $Sr_{6/5}CoO_3$, and $Sr_{14/11}CoO_3$

The magnetic properties of $Sr_{6/5}CoO_3$, $Sr_{14/11}CoO_3$, and $Sr_{9/7}NiO_3$ have not been reported so far. On the basis of the reasoning given above, we now discuss the number of spins these compounds are expected to have. In the following, we first consider that the Oh and TP site transition metal atoms of these compounds have oxidation states close to $+4$ and $+2$, respectively, and then discuss how metal–metal σ-antibonding might affect the occupations of their d-block levels.

5.1 $Sr_{9/7}NiO_3$

Each $(NiO_3)_\infty$ chain of $Sr_{9/7}NiO_3$ has one Ni_2O_9 octahedral dimer, one Ni_3O_{12} octahedral trimer, and two NiO_6 trigonal prisms (i.e., seven Ni atoms) per unit cell (Fig. 1d). The interactions between the three z^2 orbitals of the octahedral trimer lead to one σ-bonding level, one σ-nonbonding level, and one σ-antibonding level (Fig. 5b). Our calculations show that the HOMO (i.e., the highest-lying one of the nine t_{2g}-block levels) of the octahedral trimer is the nondegenerate σ-antibonding level σ_3, which lies 1.8 eV below the doubly degenerate LUMO (the lowest-lying one of the six e_g-block levels). The interactions between the two z^2 orbitals of the octahedral dimer lead to one σ-bonding and one σ-antibonding levels (Fig. 5a). Our calculations show that the nondegenerate HOMO (i.e., the highest-lying one of the six t_{2g}-block levels) of the dimer is the σ-antibonding level σ_2, which lies 1.9 eV below the doubly degenerate LUMO (the lowest-lying one of the four e_g-block levels). Of course, these pictures are valid if each $Ni^{4+}(d^6)$ cation adopts an $S = 0$ configuration. However, as discussed for the case of $Ba_{6/5}NiO_3$, the octahedral dimers and timers of $Sr_{9/7}NiO_3$ may adopt $S = 1$ configurations to reduce metal–metal σ-antibonding and electron–electron repulsion. As already discussed (Section 3.1), the $Ni^{2+}(d^8)$ cation in each NiO_6 trigonal prism may contribute effectively to about one spin. Consequently, there will be about six unpaired spins per seven Ni atoms in $Sr_{9/7}NiO_3$ if the octahedral dimers and trimers each adopt $S = 1$ configurations.

5.2. $Sr_{6/5}CoO_3$

Each $(CoO_3)_\infty$ chain of $Sr_{6/5}CoO_3$ has one Co_4O_{15} octahedral tetramer with $Co^{4+}(d^5)$ cations and one CoO_6 trigonal prism with $Co^{2+}(d^7)$ cations (i.e., five Co atoms) per unit cell (Fig. 1b). The four z^2 orbitals of the octahedral tetramer lead to two σ-bonding levels and two σ-antibonding levels (Fig. 5c). Our calculations show that the two σ-antibonding levels are the two highest-lying ones of the 12 t_{2g}-block levels of the tetramer. With $Co^{4+}(d^5)$ cation in each Oh center, the octahedral tetramer has 20 d-electrons so that the two σ-antibonding levels are not occupied. This leads to short Co–Co distances (i.e., 2.53, 2.36, 2.53 Å) in the octahedral tetramer and reduces the driving force for the tetramer to adopt an open-shell state so that the Oh cobalt atoms would be nonmagnetic. As discussed in Section 3.2, the electronic states appropriate for the TP cobalt are either the $S = \frac{1}{2}$ state Ψ_{tp} or the $S = \frac{3}{2}$ state Ψ'_{tp}. Thus, $Sr_{6/5}CoO_3$ is expected to have one and three spins per five Co atoms if each TP cobalt adopts the $S = \frac{1}{2}$ and $S = \frac{3}{2}$ states, respectively.

5.3. $Sr_{14/11}CoO_3$

Each $(CoO_3)_\infty$ chain of $Sr_{14/11}CoO_3$ has two Co_3O_{12} octahedral trimers, one Co_2O_9 octahedral dimer, and three CoO_6 trigonal prisms (i.e., 11 Co atoms) per unit cell (Fig. 1c). The two z^2 orbitals of the octahedral dimer lead to one σ-bonding level and one σ-antibonding level (Fig. 5a). Our calculations show that the σ-antibonding level is the highest-lying one of the six t_{2g}-block levels of the dimer. With a $Co^{4+}(d^5)$ cation in each Oh center, the dimer has 10 d-electrons so that the σ-antibonding level is not occupied. This leads to a short Co–Co distance (i.e., 2.40 Å) in the dimer, and the Oh cobalt atoms in the dimer would be nonmagnetic. The three z^2 orbitals of each octahedral trimer lead to one σ-bonding level, one σ-nonbonding level, and one σ-antibonding level (Fig. 5b). The σ-nonbonding and σ-antibonding levels are calculated to be the two highest-lying ones of the nine t_{2g}-block levels in the octahedral trimer. With a $Co^{4+}(d^5)$ cation in each Oh center, the trimer has 15 d-electrons so that the σ-nonbonding level is singly occupied and the σ-antibonding level is unoccupied. Thus, the Co–Co distances of the trimer are short (i.e., 2.45, 2.47 Å), and there is one spin per trimer. Thus, $Sr_{14/11}CoO_3$ is expected to have five unpaired spins per 11 Co atoms if each TP cobalt adopts that $S = \frac{1}{2}$ state Ψ_{tp}, and 11 unpaired spins per 11 Co atoms if each TP cobalt adopts the $S = \frac{3}{2}$ state Ψ'_{tp}.

6. CONCLUDING REMARKS

The two structural/electronic features of the hexagonal perovskite-type oxides A_xBO_3 are crucial for their magnetic properties, i.e., the σ orbital interactions between the z^2 orbitals of adjacent B atoms along the $(BO_3)_\infty$ chains and the doubly degenerate levels of the BO_6 polyhedra. The fact that the Ni atoms in the NiO_6 trigonal prisms of $Sr_{9/7}NiO_3$ occupy the square-planar sites as well as the positions on the 3-fold rotational axis near the trigonal prism center shows the importance of considering effective on-site repulsion and high-spin states. The observed metal–metal distances and magnetic properties of $Ba_{6/5}NiO_3$ and $Ca_{3/2}CoO_3$ imply that their structural building units adopt high-spin states to reduce the on-site repulsion as well as the σ-antibonding interactions between the z^2 orbitals. On the basis of this finding, we probed the number of unpaired spins expected for the oxides $Sr_{9/7}NiO_3$, $Sr_{6/5}CoO_3$, and $Sr_{14/11}CoO_3$. It is desirable to test the predictions of our work by experiments and first-principles calculations.

ACKNOWLEDGMENTS

Work at North Carolina State University was supported by the Office of Basic Energy Sciences, Division of Materials Sciences, U.S. Department of Energy, under Grant DE-FG05-86ER45259. K.-S.L. thanks Korea Research Foundation Grant (KRF-99-015-DP0254) for financial support.

REFERENCES

1. H. Fjellvåg, E. Gulbrandsen, S. Aasland, A. Oslen, and B. Hauback, *J. Solid State Chem.* **124,** 190 (1996).
2. J. A. Campá, E. Gutiérrez-Puebla, M. A. Monge, I. Raisines, and C. Ruiz-Valero, *J. Solid State Chem.* **108,** 230 (1994).
3. J. Darriet and M. A. Subramanian, *J. Mater. Chem.* **5,** 543 (1995).
4. W. T. A. Harrison, S. L. Hegwood, and A. J. Jacobson, *J. Chem. Soc., Chem. Commun.* 1953 (1995).
5. O. Gourdon, V. Petricek, M. Dusek, P. Bezdicka, S. Durovic, D. Gyepesova, and E. Evain, *Acta Crystallogr. B* **55,** 841 (1999).
6. M. Evain, F. Boucher, O. Gourdon, V. Petricek, M. Dusek, and P. Bezdicka, *Chem. Mater.* **10,** 3068 (1998).
7. K.-S. Lee, H.-J. Koo, D. Dai, J. Ren, and M.-H. Whangbo, *Inorg. Chem.* **38,** 340 (1999).
8. R. Gottschall, R. Schöllhorn, M. Muhler, N. Jansen, D. Walcher, and P. Gütlich, *Inorg. Chem.* **37,** 1513 (1998).
9. S. Aasland, H. Fjellvåg, and B. Hauback, *Solid State Commun.* **101,** 187 (1997).
10. H. Kageyama, K. Yoshimura, K. Kosuge, H. Mitamura, and T. Goto, *J. Phys. Soc. Jpn.* **66,** 1607 (1997).
11. H. Kageyama, K. Yoshimura, K. Kosuge, M. Azuma, M. Takano, H. Mitamura, and T. Goto, *J. Phys. Soc. Jpn.* **66,** 3996 (1997).
12. H. Kageyama, K. Yoshimura, K. Kosuge, X. Xu, and S. Kawano, *J. Phys. Soc. Jpn.* **67,** 357 (1998).
13. A. Maignan, C. Michel, A. C. Masset, C. Martin, and B. Raveau, *Eur. Phys. J. B* **15,** 657 (2000).
14. T. A. Albright, J. K. Burdett, and M.-H. Whangbo, *Orbital Interactions in Chemistry*; Wiley, New York, 1985; Chapter 2.
15. M.-H. Whangbo, *J. Chem. Phys.* **70,** 4963 (1979).
16. M.-H. Whangbo, *Inorg. Chem.* **19,** 1728 (1980).
17. R. Hoffmann, *J. Chem. Phys.* **39,** 1397 (1967).
18. J. Ren, W. Liang, and M.-H. Whangbo, "Crystal and Electronic Structure Analysis Using CAESAR," 1998; http://www.PrimeC.com/.
19. N. F. Mott, "Metal–Insulator Transitions," 2nd ed. Taylor & Francis: New York, 1990.
20. J. van Elp, R. H. Potze, H. Eskes, R. Berger, and G. A. Sawatzky, *Phys. Rev. B* **44,** 1530 (1991).
21. V. I. Anisimov, J. Zaanen, and O. K. Anderson, *Phys. Rev. B* **44,** 943 (1991).
22. V. I. Anisimov, F. Aryasetiawan, and A. I. Lichtenstein, *J. Phys.: Condens. Matter* **9,** 767 (1997).
23. K.-S. Lee, H.-J. Koo, and M.-H. Whangboo, *Inorg. Chem.* **38,** 2199 (1999).
24. H.-J. Koo and M.-H. Whangbo, *Solid State Commun.* **111,** 353 (1999).
25. M.-H. Whangbo, H.-J. Koo, and K.-S. Lee, *Solid State Commun.* **114,** 27 (2000).
26. H.-J. Koo and M.-H. Whangbo, *J. Solid State Chem.* **151,** 96 (2000).
27. M.-H.Whangbo and H.-J. Koo, *Solid State Commun.* **115,** 115 (2000).
28. H.-J. Koo and M.-H. Whangbo, *J. Solid State Chem.* **153,** 263 (2000).
29. H.-J. Koo and M.-H. Whangbo, *Inorg. Chem.* **39,** 3599 (2000).
30. M.-H. Whangbo, *Theor. Chem. Acc.* **103,** 252 (2000).
31. Y. Takeda, F. Kanamaru, M. Shimada, and M. Koizumi, *Acta Crystallogr. B* **32,** 2464 (1976).
32. M.-H. Whangbo and R. Hoffmann, *J. Am. Chem. Soc.* **100,** 6093 (1978).
33. H. Krischner, K. Torkar, and B. O. Kolbesen, *J. Solid State Chem.* **3,** 349 (1971).
34. B. Hannebauer, P. C. Schmidt, R. Kniep, N. Jansen, D. Walcher, P. Gütlich, R. Gottschall, R. Schöllhorn, and M. Methfessel, *Z. Naturforsch. A* **51,** 515 (1996).
35. C. Felser, K. Yamamura, and R. J. Cava, *J. Solid State Chem.* **146,** 411 (1999).